Polypyrrole/Ionic Liquid/Au Nanoparticle Counter-Electrodes for Dye-Sensitized Solar Cells: Improving Charge-Transfer Resistance at the CE/Electrolyte Interface

JES Focus Issue on Semiconductor Electrochemistry and Photoelectrochemistry in Honor of Krishnan Rajeshwar

Polypyrrole/Ionic Liquid/Au Nanoparticle Counter-Electrodes for Dye-Sensitized Solar Cells: Improving Charge-Transfer Resistance at the CE/Electrolyte Interface

Lara Fernandes Loguercio,[1] Carolina Ferreira de Matos,[2] Matheus Costa de Oliveira,[1] Graciane Marin,[1] Sherdil Khan,[3] Jairton Dupont,[1] Sergio Ribeiro Teixeira,[3] Naira M. Balzaretti,[3] Jacqueline F. Leite Santos,[1,z] and Marcos J. Leite Santos [1,z]

[1] *Instituto de Química, Universidade Federal do Rio Grande do Sul -UFRGS, Porto Alegre, RS, Brazil*
[2] *Universidade Federal do Pampa- UNIPAMPA Campus Caçapava do Sul, Caçapava do Sul, RS, Brazil*
[3] *Instituto de Física, Universidade Federal do Rio Grande do Sul -UFRGS, Porto Alegre, RS, Brazil*

To provide a viable alternative for counter electrodes used in dye sensitized solar cells, polypyrrole (PPy) based films have been synthesized via electrochemical deposition in the presence of the ionic liquid 1-butyl-3-methylimidazolium bis-(trifluoromethanesulfonyl) imidate (NTf_2) and incorporated with gold nanoparticles (Au_{nanop}). The films were analyzed by SEM, UV-Vis-NIR, Raman, Electrochemical impedance spectroscopy, Cyclic voltammetry and Conductivity measurements. The presence of the ionic liquid is found to result in a more conductive film, to improve catalytic reduction of I_3^- and the electrochemical reversibility of the electrode. In addition to increase conductivity, impedance spectroscopy has shown that incorporating Au_{nanop} in the PPy/NTf_2 film helps improving the interfacial charge transportation, the electrocatalytic properties and solar energy conversion efficiency. DSSCs assembled with PPy based CE presented nearly the same J-V characteristic parameters as observed from conventional Pt based device.
 [DOI: 10.1149/2.0271905jes]

Manuscript submitted October 17, 2018; revised manuscript received January 8, 2019. Published February 2, 2019. *This paper is part of the JES Focus Issue on Semiconductor Electrochemistry and Photoelectrochemistry in Honor of Krishnan Rajeshwar.*

Dye-sensitized solar cell (DSSC) is certainly one of the most promising technologies to efficiently contribute to an energy matrix, mainly based on renewable and clean approaches.[1,2] The basic structure of a DSSC is composed of a high surface area photoelectrode, an ion transport electrolyte containing a redox couple and an efficient counter-electrode presenting the ability to allow fast reduction of the redox pair.[3–5]

Previous studies have shown that photoexcited electrons must overcome a series of resistances through the device in order to generate energy output, and charge-transfer resistance at the counter electrode|electrolyte interface is often dominant. The most common material used in the counter-electrode is platinum,[6] however a growing interest is given to the development of Pt-free or low-Pt content counter-electrodes that minimize charge-transfer resistance, in addition to present low cost and easy fabrication process. The most widely reported materials as potential Pt substitutes are transition metal compounds, alloys, carbonaceous materials and conductive polymers.[7–12] Congiu et al. have assembled DSSCs using CoS counter-electrodes obtaining conversion efficiency close to Pt-based DSSCs.[7] Tsai et al. obtained conversion efficiency of 7.9% from graphene oxide based counter electrodes.[8] Conducting polymers are very interesting candidates, and have presented improved performance when incorporated with transition metal compounds.[11] Among the conducting polymers, PPy is of special interest due of its easy and low cost synthetic routes, high conductivity, good stability, high specific capacitance and optical transparency in visible-light region. In addition, PPy thin films can be porous in nature, which favors ion diffusion, increases the catalytic activity for I_3^- reduction and charge-transfer ability. One of the main processes to obtain films of PPy is electrochemical deposition. Through this approach, homogeneous thin films can be obtained, allowing the incorporation of different materials, which present optical, structural and electronic properties highly dependent on the oxidation state of the conducting polymer.[9] Previous studies have shown that ionic liquid based polymerization is a potential strategy to tune the oxidation states of conducting polymers.[11,12] In addition, the incorporation of metallic nanoparticles is found beneficial to maintain the electrical contact to the electrolyte species and to make the films electroactive for different redox reactions.[13] Hence, the combination of ionic liquid with metallic nanoparticles in electrochemically polymerized PPy seems very promising to improve conductivity and electroactivity. The current study addresses; the electrochemical polymerization of PPy films in 1-butyl-3-methylimidazolium bis-(trifluoromethanesulfonyl) imidate (BMI.NTf_2) embedded with Au_{nanop}, the modulation of PPy oxidation levels and the application of PPy based counter electrodes to replace platinum nanoparticles in DSSCs.

Experimental

Materials.—Pyrrole (Py), 1-butyl-3-methyl imidazolium methanesulfonate ($C_9H_{18}N_2O_3S$), lithium bis-(trifluoromethane sulfonyl) imide ($C_2F_6LiNO_4S_2$), dichloromethane (CH_2Cl_2), anhydrous sodium sulfate (Na_2SO_4), Gold(III) chloride trihydrate ($HAuCl_4.3H_2O$), sodium citrate ($C_6H_5Na_3O_7$), lithium iodide (LiI), iodine (I_2), 1-butyl-3-methylimidazolium iodide ($C_8H_{15}IN_2$), guanidine hydrochloride ($NH_2C(=NH)NH_2.HCl$), 4-ter-butylpyridine ($C_9H_{13}N$) and acetonitrile (CH_3CN) were obtained from Aldrich. Anhydrous lithium perchlorate ($LiClO_4$) (Dinâmica). Pyrrole was distilled and stored at ca. 4°C. 1-methylimidazole was distilled under reduced pressure. All other reagents were used without further purification.

Synthesis of 1-Butyl-3-methylimidazolium bis-(trifluoromethanesulfonyl) imidate.—1-Butyl-3-methyl imidazolium methanesulfonate (93.6 g, 0.40 mol) and lithium bis-(trifluoromethanesulfonyl) imidate (126.3g, 0.440 mol) were mixed with deionized water (210 mL), the resulting biphasic mixture was stirred for 40 min at room temperature and 400 mL of dichloromethane was added. The organic phase was separated, washed with water (4 × 50 mL), dried with anhydrous sodium sulfate and filtered. Solvent evaporation and drying under reduced pressure afforded the desired 1-butyl-3-methylimidazolium bis-(trifluoromethanesulfonyl) imidate (BMI.NTf2) as a colorless liquid (164.25g, 98%). 1H NMR (400 MHz, CDCl3) δ 8.64 (s, 1H), 7.39 (t, J = 2.0 Hz, 1H), 7,36 (t, J = 2.0 Hz, 1H), 4,17 (t, J = 7.6 Hz, 3H), 3.93 (s, 3H), 1.85 (qui, 2H), 1,37 (sex, J = 7.6 Hz, 2H), 0.95 (t, J = 7.6 Hz, 3H). 13C NMR (101 MHz, CDCl3): d ppm δ 135.64, 123.68, 122.37, 119.70 (q, JC-F = 320 Hz, CF3), 49.76, 36.06, 31.78, 19.16, 13.00.

[z]E-mail: jacqueline.ferreira@ufrgs.br; mjls@ufrgs.br

Synthesis of gold nanoparticles.—Au_{nanop} were prepared according to Turkevich method.[14] 1 mmol L^{-1} of $HAuCl_4.3H_2O$ aqueous solution (100 mL) was refluxed at 120°C under vigorous stirring, in a silicone bath. 10 mmol L^{-1} $C_6H_5Na_3O_7$ (2.5 mL) was quickly added to the reaction vessel. A sudden color change from pale yellow to red indicated the synthesis of the Au_{nanop}.

Preparation of PPy/ $LiClO_4$, PPy/ NTf_2 and PPy/ NTf_2/Au_{nanop} CEs.—The electropolymerization of the films (electrodes) was carried out at room temperature in a galvanostat/potentiostat Autolab 302N, using a conventional three-electrode cell. Fluorine doped tin oxide substrates (FTO-glass, Solaronix, 15Ω cm^{-2}) were used as working electrode, platinum plate (1 cm^2) was used as counter electrode, and Ag/AgCl was used as reference electrode. For the synthesis, the cyclic voltammetry method was performed from −0.3 to +1.3 V at a scan rate of 30 mV s^{-1}. Electrodeposition solution was prepared by dissolving 0.1 mol L^{-1} of Py in 10 mL of BMI.NTf_2, obtained (PPy/NTf_2) electrodes. PPy/NTf_2/Au_{nanop} electrodes were obtained by dipping PPy/NTf_2 in concentrated Au_{nanop} colloidal solution during 24 hours. For comparison, $LiClO_4$ doped PPy (PPy/$LiClO_4$) electrodes were synthesized using the same parameters.

DSSC assembling.—TiO_2 pastes were screen-printed on FTO previously soaked in 40 mmol L^{-1} $TiCl_4$ aqueous solution at 80°C for 30 min. The substrate was heated on a hot plate at 125°C for 20 min and at 450°C for 30 min in a tubular oven. The mesoporous TiO_2 electrode was immersed in 0.5 mmol L^{-1} *cis*-bis(isothiocyanato) bis(2,20 -bipyridyl-4,40 -dicarboxylato)-ruthenium(II) N-719 solution of acetonitrile/tertbutyl alcohol (1:1 v/v) and kept at room temperature for 24 h. Two kinds of counter-electrodes were tested: i) standard platinum based counter-electrodes prepared by coating the FTO surface with 30 μL of 1 mmol L^{-1} hexachloroplatinic acid and heating at 400°C,[15] and ii) PPy-based counter electrodes (PPy/ $LiClO_4$, PPy/ NTf_2 and PPy/ NTf_2/Aunanop). The mediator responsible for dye regeneration was placed between the dye sensitized photoanode and the counter electrode. The electrolyte was 0.6 mol L^{-1} BMII, 0.03 mol L^{-1} I_2, 0.10 mol L^{-1} guanidinium thiocyanate, and 0.5 mol L^{-1} 4-ter-butylpyridine in a mixture of acetonitrile and valeronitrile. The device was sealed using a low melting temperature polymeric film (Meltonix).

Characterization and measurements.—Morphology was studied by scanning electron microscopy (SEM) using an EVO50 Carl Zeiss microscope at 15 kV. Optical measurements were performed in a Perkin Elmer Lambda 25 spectrophotometer. Structural measurements were performed by Raman spectroscopy using an Olympus microscope, a single-pass monochromator and a charged-coupled device (CCD) detector, cooled with liquid nitrogen. Excitation was provided by 632.8 nm radiation from a 10 mW polarized He–Ne laser focused in a spot ∼2μm in diameter. Electrochemical measurements were performed in a galvanostat/potentiostat Autolab 302N. The electrocatalytic activity of I^-/I_3^- was evaluated by cyclic voltammetry within a potential range from −0.6 to +1.3V at different scan rates (20, 50, 100, 150, and 200 mV s^{-1}) and 10.0 mmol L^{-1} NaI, 1.0 mmol L^{-1} I_2, and 0.1 mmol L^{-1} of $LiClO_4$ in acetonitrile were used as electrolyte solution. The resistivities were measured directly from the films by the four-point technique using a JANDEL Universal probe. The distance between the points was fixed at 1.0 mm. DSSCs based on PPy-$LiClO_4$, PPy/NTf_2 and PPy/NTf_2/Au_{nanop} counter electrodes were characterized by current versus potential curves and electrochemical impedance spectroscopy (EIS). Profile studies were performed using a Veeco Dektak 150 equipment.

Results and Discussion

The optical properties of the PPy based electrodes were investigated by UV-Vis-NIR spectrophotometry (Figure 1). The spectra

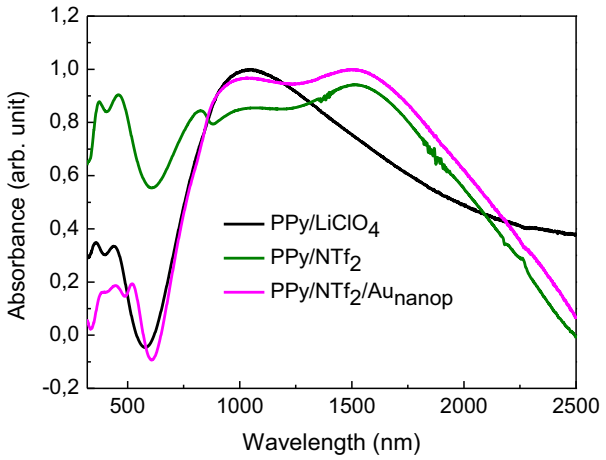

Figure 1. UV-Vis-NIR absorption spectra of the PPy based films.

present the characteristic absorptions of oxidized PPy. The bands at ca. 163 1550 nm and between 620 and 1240 nm are related to the transition from the bonding to the antibonding polaron state. The band at ca. 460 nm corresponds to the transition from the valence band to the antibonding bipolaron state, and the band at ca. 375 nm is related to the $\pi \rightarrow \pi^*$ interband transitions.[10] Among the films, polypyrrole is found in the higher oxidized state in PPy/$LiClO_4$, which is characterized by the absence of the band at 1550 nm, followed by the weakening of 890 nm band and the shift of the interband transition to higher energy.[16] As one can observe, the presence of Au_{nanop} does not change significantly the electronic structure of polypyrrole. The band at 520 nm is attributed to the presence of Au_{nanop}.

The Raman spectra of the PPy films, acquired within the range of 800–1800 cm^{-1} are shown in Figure 2. PPy/$LiClO_4$ and PPy/NTf_2 present the vibrational bands characteristic of the oxidized state at ca. 1610 cm^{-1}, related to a mixed **ν**C=C and inter-ring **ν**C-C vibration, ca. 1050, 1240, 1350, and at 930 cm^{-1}, assigned to C-H-out of the plane deformation. However, the vibration mode assigned to reduced form of the pyrrole ring, benzoid form, at ca. 980 cm^{-1}, assigned to a ring deformation mode (δ_{ring})[10,17–19] is more intense for PPy/ $LiClO_4$ hence displaying high oxidation level, as earlier observed by optical measurements (Fig. 1). The spectra intensity ratio of the bands at ca. 1050 and at ca. 1080 cm^{-1}, $A_{1050/1080}$ increased from 0.80 in PPy/$LiClO_4$ to 0.85 in PPy/NTf2 while the ratio $A_{1560/1610}$ increased from 0.68 to 0.78, showing a less oxidized PPy in the NTf_2 medium. An interesting result is the shift of the vibration mode of

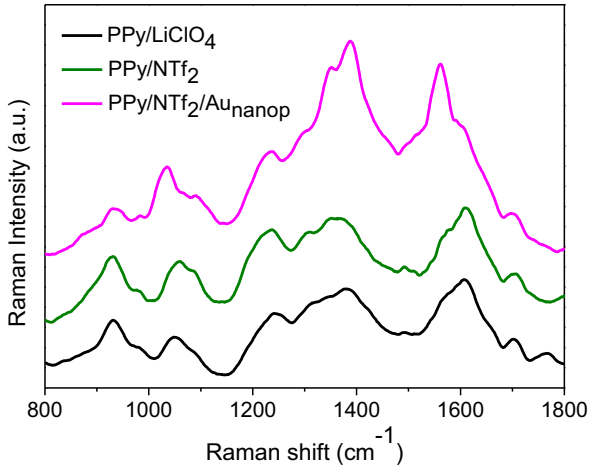

Figure 2. Raman spectra of the PPy based films. Excitation laser at 632.8 nm.

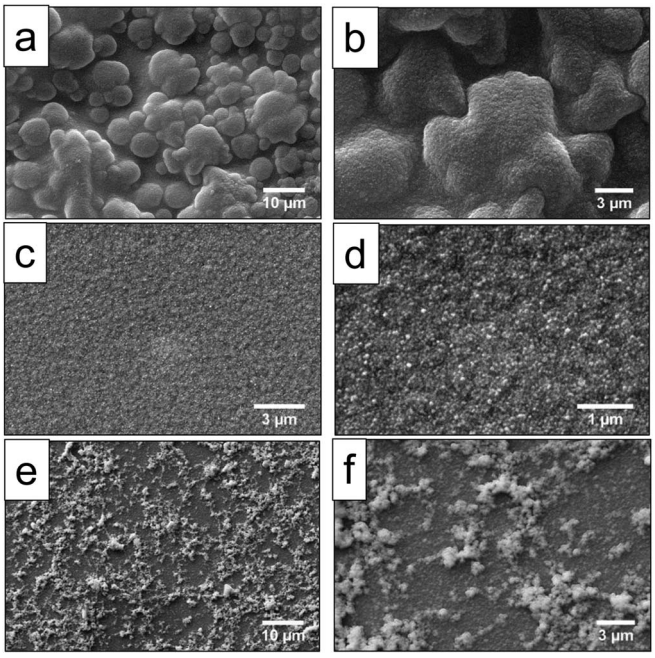

Figure 3. SEM images of PPy/$LiClO_4$ (a and b), PPy/NTf_2 (c and d) and PPy/NTf_2/Au_{nanop} (e and f).

a mixed **ν**C=C and inter-ring **ν**C-C vibration from ca. 1610 cm^{-1} to 1560 cm^{-1},[10,17–20] in PPy/NTf_2/Au_{nanop}, revealing that Au_{nanop} promote a significant reduction of the polymer chain, to a more polaronic state.[9,14] The increase in relative intensity of the vibration modes are related to surface enhanced Raman scattering.[21,22]

The SEM images of the synthesized polypyrrole films are shown in Figure 3. The surface of PPy/$LiClO_4$ consists of large granules up to 10 µm, resulting in a rough surface (1158 ± 178 nm) (Figures 3a and 3b). This morphology might be related to a high oxidation degree of PPy in PPy/$LiClO_4$, resulting from an increased number of defects in the PPy chain. PPy oxidation results in electrons removal from the chain, which leads to lattice deformation, followed by the stabilization of the cation by nearby anionic species diffused into the polymer matrix. The lattice deformation results in the loss of planarity of the chain. This geometrical distortion, although localized leads to changes in bond strengths and torsion angles that affects the ring deformation mode that consequently results in the formation of rough and irregular surface.[23,24] Once the ionic liquid is added to the electrolyte this granular rough texture changes to a much smoother surface (39 ± 20 nm) for PPy/NTf_2 film (Figs. 3c and 3d). The formation of this surface can be related to the larger portion of benzoid pyrrole rings in the PPy/NTf_2 resulting from a lower oxidation level. The presence of Au_{nanop} (PPy/NTf_2/Au_{nanop}), confirmed by EDS (not shown), makes the PPy/NTf_2 film rougher (82 ± 56 nm) (Figs. 3e and 3f). The thicknesses of the films were determined by profilometry as 3624 ± 340 nm, 373 ± 31, 192 ± 17 nm, for PPy/$LiClO_4$, PPy/NTf_2, and PPy/NTf_2/Au_{nanop} respectively. The decreasing thickness of PPy/NTf_2/Au_{nanop} can be related to the reduction of the PPy chain, as observed by Raman (Figure 2), resulting in the contraction and shrinkage of the chains.[25]

Table I. Electrochemical parameters obtained from the voltammograms presented in Figure 4b.

Electrode	E_{pa}(mV)	E_{pc}(mV)	J_{pa}(mA. cm^{-2})	J_{pc}(mA. cm^{-2})
Ppy/$LiClO_4$	530	−100	0.55	−0.31
Ppy/NTf_2	430	−6	0.70	−0.63
PPy/NTf_2/Au_{nanop}	361	−40	0.60	−0.52

The resistivity values obtained in this work (Figure 4a) are consistent with other works in the literature for electrochemically synthesized PPy films.[26–28] As earlier shown in this work, the polypyrrole in PPy/$LiClO_4$ present a higher oxidation level, hence we suggest that the lower electrical resistivity of PPy/NTf2 is related to a possible synergistic effect between PPy and the ionic liquid, improving structural ordering of the polypyrrole chains and facilitated delocalization of the charge carriers.[12] As expected the lower resistivity is obtained from PPy/NTf_2/Au_{nanop}.

Dye regeneration rate in DSSCs is controlled by the counter-electrode (CE), therefore the CE shall provide a high reduction activity for the redox pair.[29,30] Figure 4b shows the electrochemical catalytic activity, tested for I^-/I_3^-, using 10.0 mmol L^{-1} LiI, 1.0 mmol L^{-1} I_2, and 0.1 mmol $L^{-1}$of $LiClO_4$ in acetonitrile. Two pairs of redox peaks were observed for all electrodes, characteristic of I^-/I_3^- couples (a/a') and I_3^-/I_2 (b/b'). In this work, the analysis was focused on the I^-/I_3^-couple.[31,32] Table I shows the values of E*pc* and E*pa*, and current density of anodic and cathodic peaks J_{pa} and J_{pc} corresponding to the oxidation of iodide and reduction of tri-iodide ions. The potential difference between two peaks (ΔE_p) for electrodes of PPy/$LiClO_4$, PPy/NTf_2 and PPy/NTf_2/Au_{nanop} were found to be 630 mV, 436 mV and 401 mV respectively.

By comparing ΔE_p and values of current peaks from PPy/$LiClO_4$ and PPy/NTf_2 one can observe the better electrochemical catalytic ability of PPy/NTf_2. This result is related to the larger surface area that results from the homogeneous morphology and porosity, and improved conductivity of the films synthesized in ionic liquid media. These results suggest that faster electron transfer kinetics is obtained

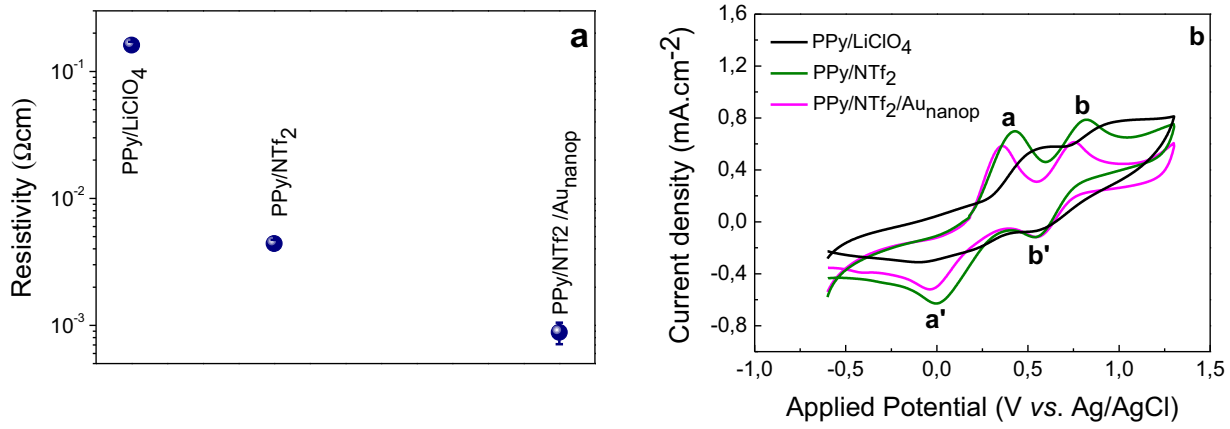

Figure 4. Four-point electrical resistivity of films (a). Voltammograms of I^-/I_3^- at a scan rate of 20 mV s^{-1} using PPy electrodes (b).

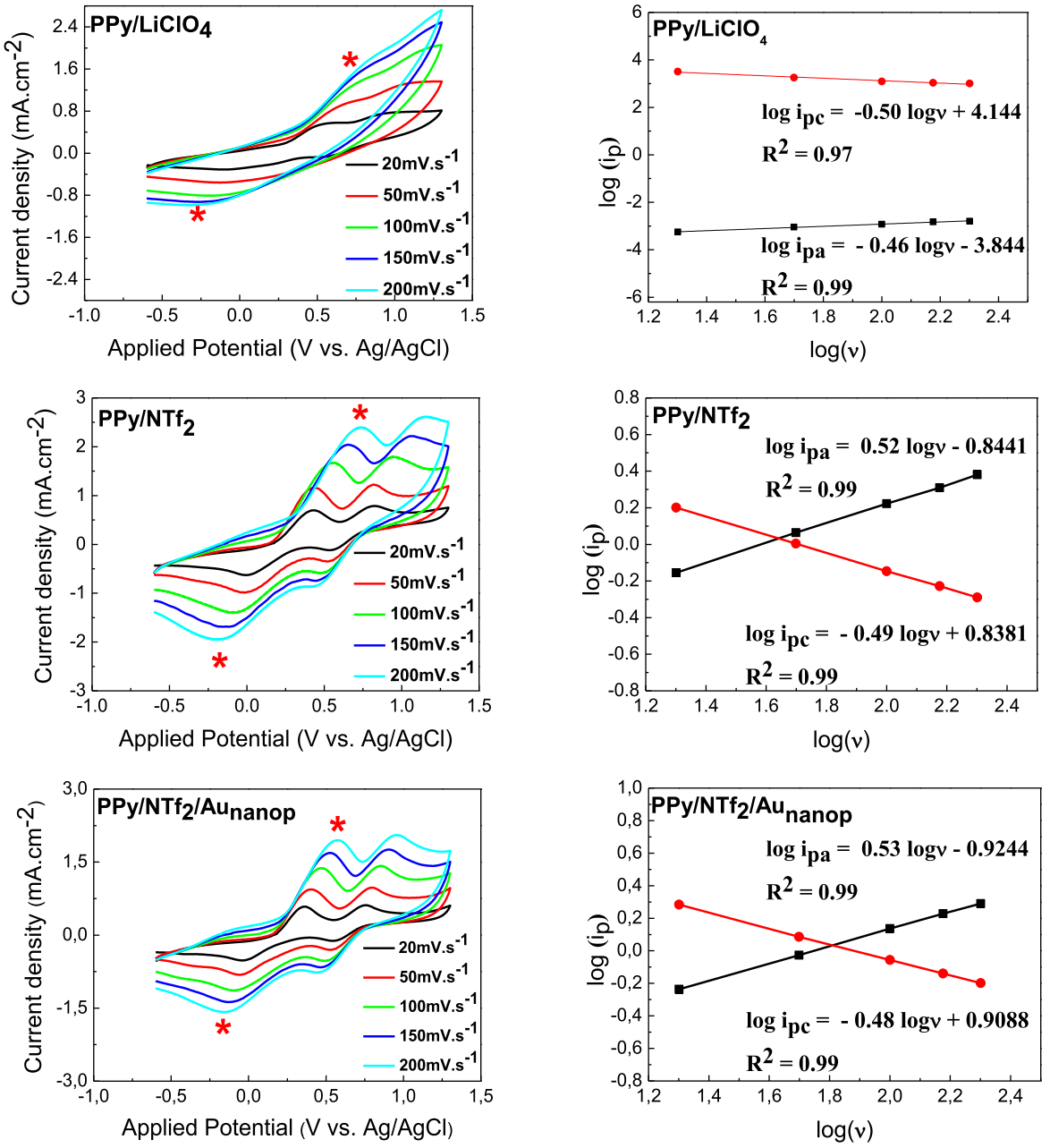

Figure 5. Voltammograms of I^-/I_3^- redox reaction at different scan rates using PPy electrodes.

when Au_{nanop} are incorporated in the film, which is related to higher catalytic activity, attributed to the active catalytic sites and increase in the conductivity of the electrode compared to PPy/NTf_2 electrode.[33,34]

The relationship between ion diffusivity, reaction kinetics and electrochemical catalytic activities were evaluated in I^-/I_3^-. Figure 5 shows the voltammograms of I^-/I_3^-redox couple at different scan rates, obtained using PPy/$LiClO_4$, PPy/NTf_2 and PPy/NTf_2/Au_{nanop}. In all electrodes, as scan rate is increased the anodic peak shifts to more positive potentials while the cathodic peak shifts toward the more negative direction. The electrodes synthesized in ionic liquid exhibit a pair of well-defined peaks for I^-/I_3^- indicating a good reversibility and catalytic activity.[35] Meanwhile, as scan rate is increased the PPy/$LiClO_4$ electrode loses reversibility, presenting less-defined peaks and the redox reaction for I_3^-/I_2 couples nearly disappear. This behavior is related to an easier oxidation of iodide than a reduction of iodine on the surface of PPy electrodes.[30] The dependence of anodic and cathodic peaks of I^-/I_3^- on the scan rate was evaluated for all electrodes by plotting the logarithm of the peak current (mA cm^{-2}) versus the logarithm of scan rate (mV s^{-1}).[35] As described by the Randles-Sevcik equation, the electrochemical behavior of the studied PPy electrodes is governed by diffusion of iodide species inside the PPy chain. As one can observe in Figure 5, the slope of the anodic curve slightly varies from 0.50 to 0.53, which indicates that the synthesized PPy based electrodes possess nearly the same electroactive surface area. Figure 6 shows the J_{pa} and J_{pc} correspondence of I^-/I_3^- and I_3^-/I_2 redox couples for different PPy electrodes during 30 consecutive cycles. These analyses exhibit linearity showing that these parameters are nearly steady after the cycles, suggesting a good electrochemical stability for I^-/I_3^- based electrolyte reaction. However, the PPy/NTf_2 electrode exhibit very well-defined peaks when compared to PPy/$LiClO_4$.[36]

Figure 7 displays the J-V curves of the DSSCs assembled with PPy counter electrodes (CEs) and for comparison a Pt based device is also evaluated (Table II). The highest fill factor (FF), open circuit potential

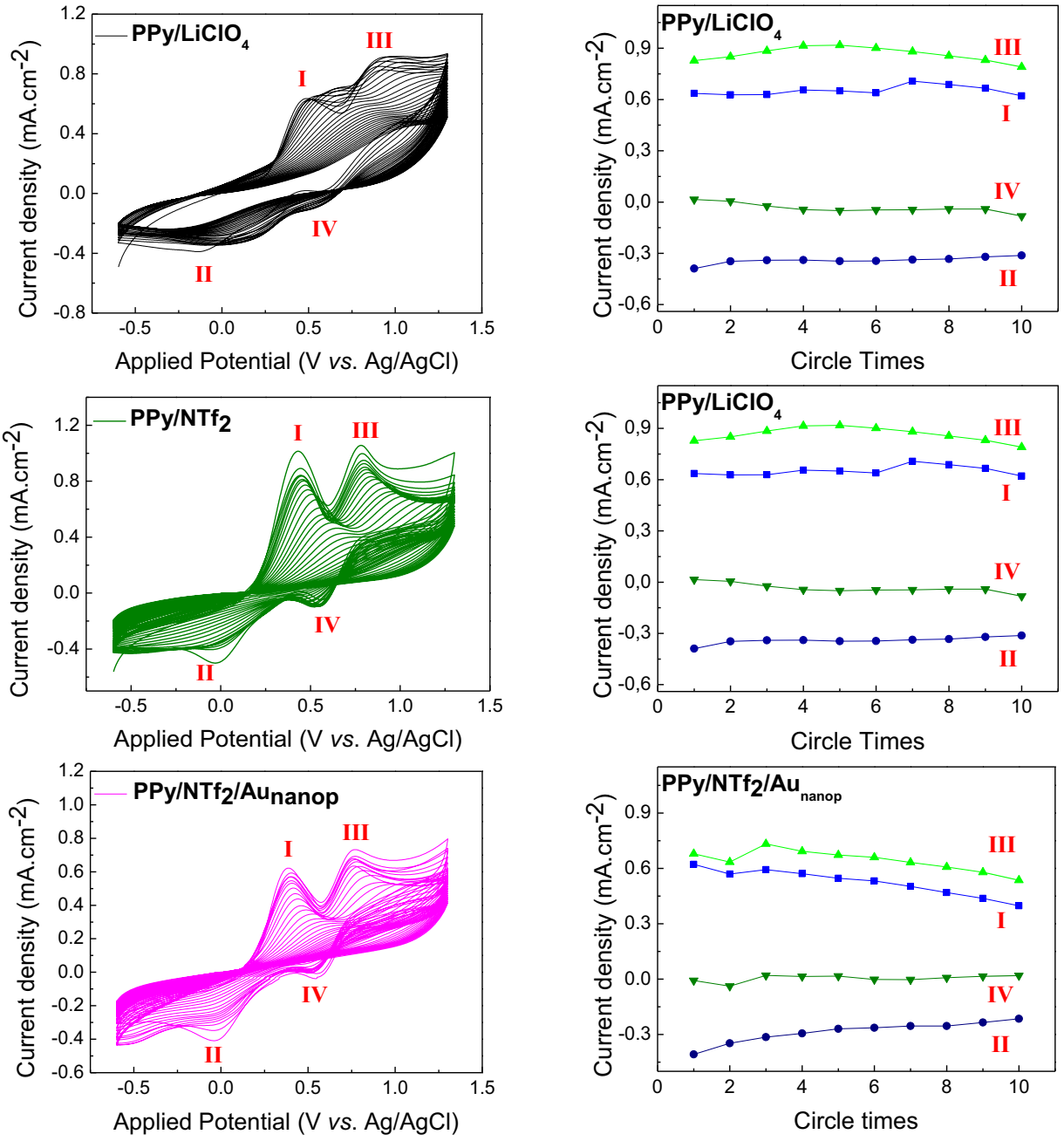

Figure 6. Consecutive cyclic voltammograms (30 cycles) of I^-/I_3^- redox reaction at a scan rate of 20 mV s^{-1} using PPy electrodes. The relationship between consecutive 10 cycle times of I^-/I_3^- redox reaction peak currents for PPy electrodes.

(V_{oc}) value and efficiency (n %) are obtained from Pt based device. In terms of FF the PPy films follow the order: $PPy/NTf_2/Au_{nanop}$ > PPy/NTf_2 > $PPy/LiClO_4$. $PPy/NTf_2/Au_{nanop}$ presents DSSC performance that is comparable to Pt and other PPy based CE reported in the literature.[36–38] Hence, doping PPy with IL and embedding Au_{nanop} in the film is a potential methodology to obtain PPy based counter electrodes applied in DSSC.

To understand the interfacial charge transportation in the devices electrochemical impedance spectroscopy (EIS) was performed. In J-V curves, $PPy/LiClO_4$ has shown lowest FF; therefore, we did not perform EIS measurements for this device. For all other devices these measurements were performed in 0.1 mol.L^{-1} $LiClO_4$ in dark (Figure 8a) and under illumination (Figure 8b). The value of the V_{oc} under illumination was chosen as the applied bias for both conditions. The starting point of the Nyquist plot is the series resistance (R_S) caused by the substrates, connecting wires, etc.; followed by a small first semicircle observed at higher frequencies with resistance R_1 which is referred to the charge transfer resistance at the CE/electrolyte interface and a larger second semicircle corresponding to the charge transfer resistance (R_2) at the electrodes/dye/electrolyte interface.[39,40] At first glance, in both experiments the real part of impedance is highest for PPy/NTf_2 and lowest for Pt based device. The data were fit to an equivalent circuit containing a combination of resistance components and constant phase elements (CPEs) as shown in the inset of Figure 8a and are presented in Table III.[41] As one can observe R_s presents a clear dependence on the counter electrode following the same trend as observed for their resistivity values (Figure 4a), in addition, it remained nearly unaffected in dark and under illumination. At V_{oc} under illu-

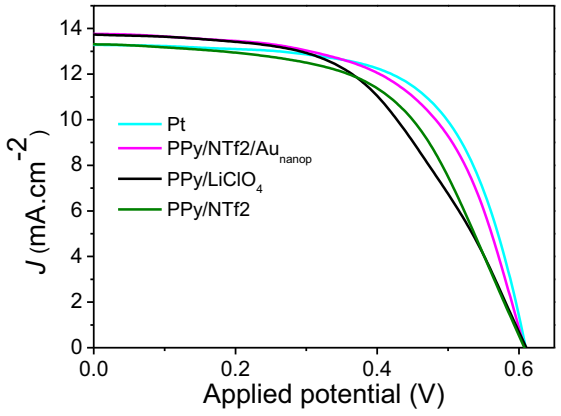

Figure 7. *J-V* curves of DSSCs using on PPy films and Pt CEs and measurements were made after 24 hours of the assembled devices.

Table II. Electrical parameters obtained from the J x V curves of the DSSCs.

CE	J_{sc} (mA. cm^{-2})	V_{oc} (mV)	FF (%)	η (%)
Pt	13.3	0.61	65	5.3
PPy/$LiClO_4$	13.7	0.60	59	4.7
PPy/NTf_2	13.2	0.61	60	4.7
PPy/NTf2/Au_{nanop}	13.7	0.60	61	5.0

mination there is no net flow of the current through the device which ensures the counter electrode is in equilibrium. At this condition, the electrons are captured by I_3^- without passing to the external circuit and hence the photon energy is mainly converted into heat. On the other hand, in dark the applied negative potential represents a forward bias at which the electrons can move through TiO_2 to react with I_3^- and oxidize I^- to I_3^-; implying the flow of net current. It can be clearly seen that under illumination both R_2 and R_3 values are smaller than those observed in dark. This result can be rationalize on the basis of higher local concentration of I_3^- under illumination which increases the photogenerated conduction band electrons capture rate and shortens the electrons life time in TiO_2; thereby decreasing the charge transfer resistances.[42] The overall resistance ($R_T = R_s + R_1 + R_2$) is a determinant parameter to the device performance. It can be seen, lowest R_T value was found for Pt based device followed by PPy/NTf_2 and PPy/NTf_2/Au_{nanop} based devices corroborating the same trend as observed in their J-V characteristics. It is important to note that once we embedded the Au_{nanop} in PPy/NTf_2; not only the J-V characteristic parameters are improved but also the interfacial resistance is decreased which might be related to the improved connectivity of Au_{nanop} to the substrate in addition to their high conductivity.[42,43] It should be noted that the PPy based devices are much more resistive than the one based on Pt CE. This might be related to different mechanisms

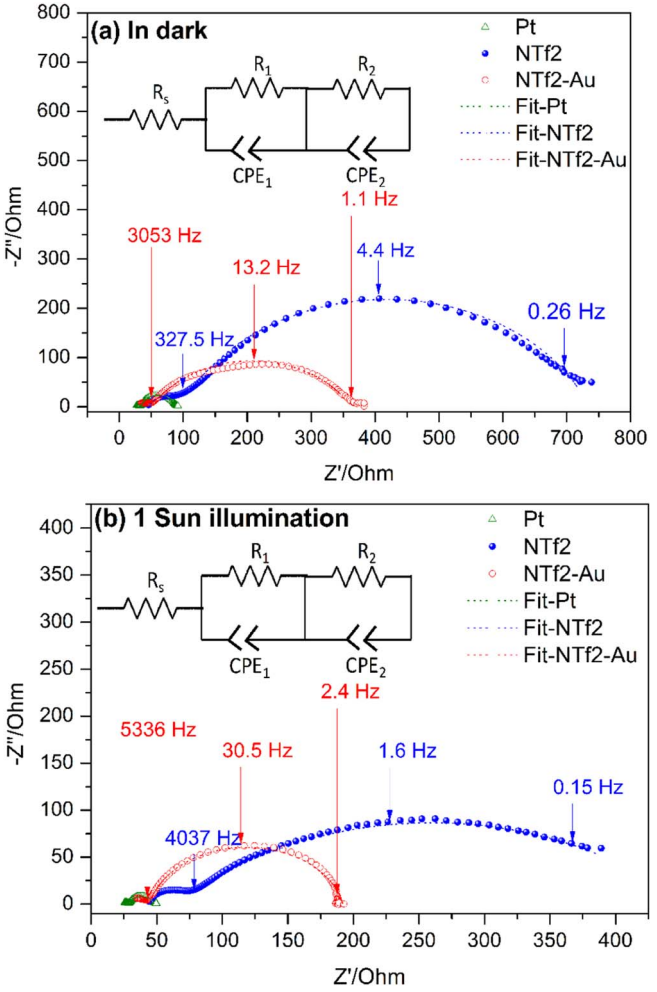

Figure 8. Nyquist plots of the assembled DSSCs: (a) in dark and (b) under illumination. The inset displays the equivalent circuit used to fit the EIS data.

related to the redox process on conducting polymers as compared to Pt e.g. ionic diffusion coefficient dependence on PPy thickness and electrolyte concentration in addition to the diffusion speed dependence on the doping level.[44,45] The electron transport within metals and at metal liquid interfaces do not differ substantially which is contrary to what is usually observed in conducting polymers.

Conclusions

In summary, we have demonstrated that electrochemical polymerization of PPy in ionic liquid can drive the oxidation state of the polypyrrole chains. The PPy based electrodes have presented a promising electrochemical and chemical reversibility for I^-/I_3^-. The

Table III. The values of the circuit elements obtained from the equivalent circuit fitting of EIS data.

			CPE$_1$			CPE$_2$			
Sample	Condition	R_s (Ω)	Q_1(μF)	n_1	R_1 (Ω)	Q_2(μF)	n_2	R_2 (Ω)	R_T (Ω)
Pt	Dark	28.1	74.4	0.74	6.1	424.7	0.74	54.3	88.5
PPy/NTf_2		45.9	15.5	0.76	56.3	169.2	0.76	633	735.2
PPy/NTf2/Au_{nanop}		39.6	25.0	0.74	11.7	151	0.74	311	362.3
	1 Sun Illum.								
Pt		26.9	30.1	0.90	2.1	547	0.90	18.6	47.6
PPy/NTf_2		43.2	9.6	0.84	23.6	897	0.85	384	450.8
PPy/NTf2/Au_{nanop}		38.8	22.2	0.79	6.3	53.7	0.79	147	192.1

performance of the DSSCs using PPy-based counter electrodes was governed by the morphology, conductivity and electrocatalytic properties of the PPy films, while these properties were ultimately controlled by the presence of the ionic liquid. PPy/NTf2/Au_{nanop} films are porous in nature, environment friendly, present low vapor pressure, low cost and high electrocatalytic activity for iodide/triiodide. All these characteristics make this material very interesting for application as counter electrodes for DSSC. However, the PPy based electrodes present low catalytic stability and new efforts are required to further improve their electrochemical properties in comparison to Pt.

Acknowledgments

The authors gratefully acknowledge funding support, scholarships, and fellowships from Conselho Nacional de Desenvolvimento Científico e Tecnológico (CNPq), Brazil, and Coordenacão de Aperfeiçoamento de Pessoal de Nível Superior (CAPES). They are thankful to Center of Microscopy (CME-UFRGS) for the SEM images.

ORCID

Marcos J. Leite Santos https://orcid.org/0000-0002-3347-9092

References

1. J. Gong, K. Sumathy, Q. Qiao, Z. Zhou, and Z. Zhengping, *Renew Sust Energ Rev*, **68**(1), 234 (2017).
2. M. Ye, X. Wen, M. Wang, J. Locozzia, N. Zhang, C. Lin, and Z. Lin, *Mater Today*. **18**, 155 (2015).
3. L. Shan, W. Shasha, H. Ruobing, F. Ting, G. Lingju, Z. Xuehua, L. Dongsheng, and H. Tao, *J. Mater Chem A*, **2**, 12805 (2014).
4. S. Mathew, A. Yella, P. Gao, R. Humphry-Baker, B. F. Curchod, N. Ashari-Astani, I. Tavernelli, U. Rothlisberger, Md. K. Nazeeruddin, and M. Grätzel, *Nat Chem*. **6**, 242 (2014).
5. X. Jie, L. Meixia, W. Lei, S. Yongyuan, Z. Ligen, G. Shaojin, L. Li, B. Zikui, F. Dong, and X. Weilin, *J. Power Sources*, **257**, 230 (2014).
6. J. Wu, Q. Li, L. Fan, Z. Lan, P. Li, J. Lin, and S. Hao, *J. Power Sources*. **181**, 172 (2008).
7. M. Congiu, M. Bonomo, M. L. De Marco, D. P. Dowling, A. Di Carlo, D. Dini, and C. F. O. Graeff, *Chemistry Select*, **16**, 2808, (2016).
8. C-H. Tsai, S-L. Shiu, W-C. Lin, Y-R. Chou, and Y-H. Yu, *Organic Electronics*, **64**, 166, (2019).
9. M. J. L. Santos, A. Brolo, and E. Girotto, *Electrochim Acta*, **52**, 6141 (2007).
10. J. L. Brédas, R. Silbey, D. Boudreaux, and R. Chance, *J. Am Chem Soc*, **105**, 6555 (1983).
11. S. Pitchaimuthu, R. Vedarajan, K. L. V. Joseph, and Y. S. Kang, Chapter 10, 2018. https://doi.org/10.1002/9783527813636.ch10.
12. L. F. Loguercio, C. F. Matos, M. C. Oliveira, G. Marin, S. Khan, N. M. Balzaretti, J. DuPont, M. J. L. Santos, and J. F. L. Santos, *New J. Chem*, **42**, 13828 (2018).
13. P. S. Kishore, B. Viswanathan, and T. K. Varadarajan, *Nanoscale Res Lett*, **3**(1), 14 (2008).
14. B. V. Enustun and J. Turkevich, *J. Am Chem Soc*, **85**, 3317 (1963).
15. S. Ito, T. N. Murakami, P. Comte, P. Liska, C. Grätzel, M. K. Nazeeruddin, and M. Grätzel, *Thin Solid Films*, **516**, 4613 (2008).
16. K. Yakushi, L. J. Lauchlan, T. C. Clarke, and G. B. Street, *J. Chem Phys*, **79**, 4774 (1983).
17. F. Chen, G. Shi, M. Fu, L. Qu, and X. Hong, *Synth Met*, **132**(2), 125 (2003).
18. C. M. Jenden, R. G. Davidson, and T. G. Turner, *Polymer*, **34**(8), 1649 (1993).
19. J. Scott, J. Bredas, K. Yakushi, P. Pfluger, and G. Street, *Synth Met*, **9**(2), 165 (1984).
20. J. L. Bredas and G. B. Street, *Polarons, bipolarons, and solitons in conducting polymers. Acc Chem Res*, **18**(10), 309 (1985).
21. T. C. Chuang, Y. C. Liu, and C. C. Wang, *J Raman Spectrosc*, **36**(6), 704 (2005).
22. W. Chen, C. M. Li, P. Chen, and C. Q. Sun, *Electrochim Acta*, **52**(8) 2845 (2007).
23. J. L. Bredas, R. R. Chance, and R. Silbey, *Phys Rev B*, **26**, 5843 (1982).
24. E. Yurtsever and M. Yourtsever, *Synth Met*, **101**, 335 (1999).
25. T. F. Otero and M. T. Cortés, *Sensors and Actuators B*, **96**, 152 (2003).
26. M. Deepa and S. Ahmad, *Eur Polym J*, **44**, 3288 (2008).
27. J. Park, S. Lee, B. Kim, and Y. Park, *Appl Phys Lett*, **81**, 4625 (2002).
28. L. Yuan, B. Yao, B. Hu, K. Huo, W. Chen, and J. Zhou, *Energy Environ Sci*, **6**, 470 (2013).
29. J. Wu, Z. Lan, J. Lin, M. Huang, Y. Huang, L. Fan, G. Luo, Y. Lin, Y. Xie, and Y. Wei, *Chem Soc Rev*, **46**, 5975 (2017).
30. S. Lu, S. Wang, R. Han, T. Feng, L. Guo, X. Zhang, D. Liu, and T. He, *Mater Chem A*, **2**, 12805 (2014).
31. B. B. Carbas, M. Gulen, M. C. Tolu, and S. Sonmezoglu, *Sci Rep*, **7**, 1 (2017).
32. M. Bonomo, A. Di-Carlo, and D. Dini, *Journal of The Electrochemical Society*, **165**(14), H889 (2018).
33. X. Pan, K. Zhu, G. Ren, N. Islam, J. Warzywoda, and Z. Fan, *J Mater Chem A*, **2**, 12746 (2014).
34. X. Zhang, S. Wang, S. Lu, J. Su, and T. He, *J Power Sources*. **246**, 491 (2014).
35. L. F. Loguercio, P. Demingos, L. M. Manica, J. B. Griep, M. J. L. Santos, and J. Ferreira, *Journal of Chemistry*, **1**, 1 (2016).
36. S. P. Lim, A. Pandikuma, S. Y. Lim, N. M. Huang, and N. H. Lim, *Sci Rep*, **4**, 1. (2014).
37. W. Houa, Y. Xiaoa, G. Hana, and Z. Haihan, *Electrochim Acta*, **190**, 720 (2016).
38. T. Peng, W. Sun, C. Huang, W. Yu, B. Sebo, Z. Dai, S. Guo, and Z. Zhao, *Appl. Mater. Interfaces*, **6**, 14 (2014).
39. T. Hoshikawa, T. Ikebe, R. Kikuchi, and K. Eguchi, *Electrochim. Acta*, **51**, 5286 (2006).
40. X. Sun, Y. Liu, Q. Tai, B. Chen, T. Peng, N. Huang, S. Xu, T. Peng, and X.-Z. Zhao, *J. Phys Chem C*, **116**(22), 11859 (2012).
41. E. C. Kohlrausch, M. J. M. Zapata, R. V. Gonçalves, S. Khan, M. O. Vaz, J. DuPont, S. R. Teixeira, and M. J. L. Santos, *RSC Adv*, **5**, 101276 (2015).
42. W. Chen, C. M. Li, P. Chen, and Q. C. Sun, *Electrochim Acta*, **52**, 2845 (2007).
43. C. H. Lia, C. P. Leea, M. S. Fana, P. Y. Chena, R. Vittala, and K. Ho, *Nano Energy*. **9**, 1 (2014).
44. J. M. Pernaut, L. C. Soares, and J. C. Belchior, *J. Braz. Chem. Soc.*, **8**(2), 175 (1997).
45. Alan J. Heeger, *Faraday Discuss. Chem. SOC.*, **88**, 203 (1989).